EUROFUSION WPJET1-PR(16) 15391

L Frassinetti et al.

Dimensionless scans in low baseline JET-ILW plasmas and comparison with JET-C

Preprint of Paper to be submitted for publication in
43rd European Physical Society Conference on Plasma Physics (EPS)

This work has been carried out within the framework of the EUROfusion Consortium and has received funding from the Euratom research and training programme 2014-2018 under grant agreement No 633053. The views and opinions expressed herein do not necessarily reflect those of the European Commission.

This document is intended for publication in the open literature. It is made available on the clear understanding that it may not be further circulated and extracts or references may not be published prior to publication of the original when applicable, or without the consent of the Publications Officer, EUROfusion Programme Management Unit, Culham Science Centre, Abingdon, Oxon, OX14 3DB, UK or e-mail Publications.Officer@euro-fusion.org

Enquiries about Copyright and reproduction should be addressed to the Publications Officer, EUROfusion Programme Management Unit, Culham Science Centre, Abingdon, Oxon, OX14 3DB, UK or e-mail Publications.Officer@euro-fusion.org

The contents of this preprint and all other EUROfusion Preprints, Reports and Conference Papers are available to view online free at http://www.euro-fusionscipub.org. This site has full search facilities and e-mail alert options. In the JET specific papers the diagrams contained within the PDFs on this site are hyperlinked

Dimensionless scans in low triangularity baseline plasmas in JET-ILW

L. Frassinetti[1], S. Saarelma[2], P. Lomas[2], I. Nunes[3], F. Rimini[2], M. N. A. Beurskens[4], P. Bilkova[10], J. E. Boom[5], E. de la Luna[6], E. Delabie[7], P. Drewelow[2], J. Flanagan[2], L. Garzotti[2], C. Giroud[2], N. Hawks[2], E. Joffrin[2], M. Kempenaars[2], Hyun-Tae Kim[2], U. Kruezi[2], A. Loarte[8], B. Lomanowski[9], I. Lupelli[2], L. Meneses[3], C.F. Maggi[2], S. Menmuir[2], M. Peterka[10], E. Rachlew[11], M. Romanelli[2], E. Stefanikova[1], and JET contributors*

EUROfusion Consortium, JET, Culham Science Centre, Abingdon, OX14 3DB, UK
[1]Division of Fusion Plasma Physics, KTH Royal Institute of Technology, SE-10691 Stockholm, Sweden
[2]CCFE, Culham Science Centre, Abingdon,OX14 3DB, UK
[3]Instituto de Plasmas e Fusão Nuclear, IST, Universidade de Lisboa, 1049-001 Lisboa, Portugal
[4]Max-Planck-Institut für Plasmaphysik, D-17491 Greifswald, Germany
[5]Max-Planck-Institut für Plasma Physik, Boltzmannstr.2, 85748 Garching, Germany
[6]Laboratorio Nacional de Fusión, CIEMAT, 28040, Madrid, Spain
[7]Oak Ridge National Laboratory, Oak Ridge, TN 37831-6169 USA
[8]ITER Organization, Plasma Operation Directorate, 13115 St Paul Lez Durance, France
[9]Aalto University, TEKES, Espoo, Finland
[10]Institute of Plasma Physics AS CR vvi, Prague, Czech Republic
[11]Department of Physics, KTH Royal Institute of Technology, SE-10691 Stockholm, Sweden
** See the Appendix of F. Romanelli et al., Proceedings of the 25th IAEA Fusion Energy Conference 2014, Saint Petersburg, Russia*

Abstract

Three dimensionless scans in the normalized Larmor radius ρ^*, normalized collisionality ν^* and normalized plasma pressure β have been performed in JET with the ITER-like wall (JET-ILW).

The normalized energy confinement and the thermal diffusivity exhibit a scaling with ρ^* consistent with the earlier results obtained in the carbon wall JET (JET-C) and with a gyro-Bohm scaling. In the pedestal, experimental results show that the stability is not dependent on ρ^*, qualitatively in agreement with the peeling-ballooning (P-B) model.

The ν^* dimensionless scaling shows that JET-ILW normalized confinement has a stronger dependence on collisionality than JET-C. This leads to a reduction of the difference in the confinement between JET-ILW and JET-C to $\approx$10% at low ν^*. The pedestal stability shows an improvement with decreasing ν^*. This is ascribed to the increase of the bootstrap current, to the reduction of the pedestal width and to the reduction of the relative shift between pedestal density and temperature position.

The β dimensionless scan shows that, at low collisionality, JET-ILW normalized confinement has no clear dependence with β, in agreement with part of the earlier scalings. At high collisionality, a reduction of the normalized confinement with increasing β is observed. This behaviour is driven by the pedestal where the stability is reduced with increasing β. The P-B analysis shows that the stability reduction with increasing β at high ν^* is due to the destabilizing effect of the increased relative shift.

1. INTRODUCTION

Dimensionless scalings in plasma physics are recognized as an important technique to extrapolate the plasma performance to future fusion machines such as ITER and to compare different tokamak experiments [Luce PPCF2008]. Dimensionless scalings can also provide useful information to discriminate between the different types of transport and physics models that have been proposed to describe the plasma confinement. If the energy transport is determined by plasma physics, it can be shown [Connor NF1977] that the normalized energy confinement time is determined by a set of dimensionless parameters [Kadomstev SJPP1975]:

$$\tau_E/\tau_B=F(\rho^*,\nu^*,\beta^{th},M_{rot},T_e/T_i,Z_{eff},q,\varepsilon,k,\delta,\ldots) \quad (1)$$

where τ_E is the thermal energy confinement, $\tau_B = a^2B/T$ is the Bohm confinement time (with a the minor radius, B the magnetic field and T the temperature). ρ^* is the ion Larmor radius:

$$\rho^* = \frac{\sqrt{2Am_pT_i}}{eBa} \quad (2)$$

with A the mass number, m_p the proton mass, T_i the ion temperature and e the electric charge. ν^* is the normalized collisionality defined as the ion-electron collision rate normalized to the thermal ion bounce frequency as in [Sauter PoP2002]:

$$\nu^* = 6.91 \cdot 10^{-18} \frac{Rq_{95}Z_{eff}ln\Lambda}{\varepsilon^{3/2}T_e^2} \quad (3)$$

with R the major radius, q the safety factor, Z_{eff} the effective charge, ε is the inverse aspect ratio, T_e the electron temperature and $\ln\Lambda$ the Coulomb logarithm. This collisionality definition is used in the present work because of its role in the bootstrap current [Sauter PoP2002] and hence in the pedestal stability. β^{th} is the normalized thermal pressure:

$$\beta^{th} = \frac{(p_e+p_i)}{B^2/\mu_0} \quad (4)$$

with p_e and p_i the electron and ion thermal pressure respectively. M_{rot} is the Mach number of the plasma rotation, $M_{rot}=v/v_{th}$, with v is the plasma velocity and $v_{th}=\sqrt{eT_i/m}$ is the thermal velocity [De Vries PPCF2006]. Finally, δ the triangularity. Note that an expression similar to equation 1 holds for the thermal plasma diffusivity χ normalized to the Bohm diffusion coefficient $\chi_B=kT/eB$.

The scaling of the normalized energy confinement described by equation (1) can be rewritten using the Connor-Taylor invariance argument [Connor NF1977] by expressing the dependence with each dimensionless parameter as a power law: $\tau_E/\tau_B \propto \rho^{*-\alpha_\rho}\, \nu^{*-\alpha_\nu}\, \beta^{-\alpha_\beta}$ ... For simplicity, most of the dimensioness scaling analysis expresses τ_B and χ as a function of ρ^* and B, therefore obtaining the expressions:

$$B\tau_E \propto \rho^{*-(2+\alpha_\rho)}\, \nu^{*-\alpha_\nu}\, \beta^{-\alpha_\beta}\, q^{-\alpha_q} Z_{eff}^{-\alpha_z} M_{rot}^{-\alpha_M} \ldots \quad (5)$$

$$\chi/\mathrm{B} \propto \rho^{*2+\alpha_\rho}\, \nu^{*\alpha_\nu}\, \beta^{\alpha_\beta}\, q^{\alpha_q} Z_{eff}^{\alpha_z} M_{rot}^{\alpha_M} \ldots \quad (6)$$

One of the goals of the dimensionless scaling experiments is to estimate the exponents of the power laws in expressions (5)-(6). Dimensionless scaling experiments consist in varying one dimensionless parameter while keeping the other constant. In a specific machine and for plasmas with same minor radius, major radius, elongation and delta, the transport and the confinement can be described by the four dimensionless parameters ρ^*, ν^*, β and M_{rot}. The values of the exponents not only are useful for extrapolations to future machines but also carry useful information on the type of transport that regulates the plasma confinement. This is briefly summarized in the following part of the section, along with a concise overview of earlier results (further detailed information can be found in reference [Luce PPCF2008]).

I. The ρ*-scaling exponent carries information on the type of turbulent transport in the core. For example, $B\tau_E \approx \rho^{*-3}$ implies a gyro-Bhom scaling, $B\tau_E \approx \rho^{*-2}$ implies a Bhom scaling and $B\tau_E \approx \rho^{*-1}$ implies that the transport is dominated by a stochastic magnetic field. Experimental results performed in most of the machines agree with a gyro-Bhom scaling type for H-mode plasmas [Petty PoP1995, Ryter IAEA1996, Greenwald PPCF1998, Shirai PPCF2000]. Specifically, the scaling $B\tau_E \approx \rho^{*-2.7}$ has been obtained in JET-C [Cordey NF2005, Nunes NF2013]. These results are consistent with the IP98(y,2) scaling which expects $B\tau_E \approx \rho^{*-2.7}$ [ITER NF1999a].

II. The collisionality is believed to have a strong influence on the turbulence. At high ν* the trapped electron modes (TEMs) are stabilized [Angioni PoP2005] while the ion temperature gradient (ITG) modes are destabilized [Falchetto PRL2004] leading respectively to a reduction and an increase of the transport with collisionality. Experimental results in DIII-D H-mode plasmas show the increase of the transport with increasing ν*, with the exponent in the range $\alpha_\nu \approx +0.35/+0.56$ [Petty PoP1999]. JET-C and JT60-U have obtained results consistent with the DIII-D estimations with $\alpha_\nu = 0.35 \pm 0.04$ in JET-C [McDonald IAEA2004, Shirai PPCF2000]. In MAST, the improvement with decreasing collisionality is even stronger, with $\alpha_\nu = 0.82 \pm 0.01$ [Valovic NF2011]. Note that these results are different from the IP98(y,2) scaling which shows no dependence of the normalized confinement versus ν*, with an exponenent $\alpha_\nu = -0.01$.

III. The β-scaling exponent helps in discriminating between the transport dominated by electrostatic turbulence and electromagnetic turbulence. A strong dependence with β suggests a core turbulent transport dominated by electromagnetic effects, while weak or no dependence suggests a core turbulent transport dominated by electrostatic effects.

Experimental results on both DIII-D [Petty PoP2004] and JET-C [McDonald PPCF2004] show a very weak dependence, with α_β=0.01±0.11 in JET-C. On the other hand, results obtained in JT-60U and ASDEX Upgrade show a degradation of the normalized confinement with β: $\alpha_\beta\approx0.6$ [Urano NF2006] and $\alpha_\beta\approx0.9$ [Vermare NF2007]. An unfavourable dependence with β has been observed also in MAST and NSTX [Kaye PPCF2006]. The IPB98(y,2) scaling as well shows a strong degradation of the normalized confinement with $\alpha_\beta\approx0.9$.

Dimensionless scaling experiments for M_{rot} in H-mode plasmas are very challenging and, to the knowledge of the authors, no results on the M_{rot} exponenent are available from a dimensionless scan. For JET-C the only available result is obtained from a large dataset containing various operational scenarios [de Vries NF2008]. The scaling is $\tau_E\approx M_{rot}^{0.21}$ but it refers to the global energy confinement, not to the normalized energy confinement. A discussion on the possible impact of M_{rot} in the present datasets is presented in Section 2.3.

Even if several experiments have already studied the dependence of the plasma transport and confinement with dimensionless parameters, it is important to extend these studies to JET with the ITER-like wall (JET-ILW). There are two main reasons.

(1) JET-ILW low β_N plasmas (with $\beta_N\lesssim1.8$, the so-called "baseline" scenario) tend to have energy confinement lower than the corresponding JET plasmas produced with the earlier carbon wall (JET-C plasmas) [Beurskens NF2014, Nunes PPCF2016]. There is concern that the difference could imply a modification of the presently determined dimensionless scaling laws and hence of the prediction for ITER obtained from the IPB98(y,2) scaling [ITER NF1999a]. This is particularly important for the normalized ion Larmor radius scaling ρ*, for the normalized collisionality ν* and for the normalized thermal pressure. (1a) Recent results [Nunes PPCF2016] show that the increase in plasma current has, so far, led to a reduction of H_{98} in JET-ILW. Here H_{98} is the ratio between the thermal energy confinement and the confinement expected by the IPB98(y,2) scaling. Since $H_{98}=1$ implies $B\tau_E\approx\rho^{*-2.7}$ [ITER NF1999b], a degradation of H_{98} with increasing plasma current might suggest a weaker ρ* scaling in JET-ILW. For reliable ITER predictions, it is vital to determine if the metal wall has, somehow, modified the ρ* scaling. (1b) The results of the first JET-ILW campaign [Beurskens NF2014] have shown that the JET-ILW low δ baseline plasmas tend to reach confinement close to the corresponding JET-C plasmas at low collisionality. So, it is important to verify if and why a different scaling with ν* is present with the metal wall. (1c) High β operations are attractive due to the positive scaling of the fusion power with β. But no

consensus on the β scaling of the normalized energy confinement has been reached [Petty PoP2004, McDonald PPCF2004, Urano NF2006, Vermare NF2007].

(2) Most of the earlier dimensionless scans were focused on the global energy confinement and on the core thermal transport. On the other hand, the pedestal plays a major role in determining the stored energy of an H-mode plasma. So far, the pedestal structure has been investigated in terms of dimensionless scalings in few works, see for example the ρ* scaling in JET-C, DIII-D and ASDEX Upgrade [Beurskens PoP2011, Ryter IAEA1998]. The pedestal stability has not been studied yet in detail in terms of dimensionless scalings. Assessing experimentally the dependence of the pedestal structure on the dimensionless parameters and qualitatively testing the present pedestal models are vital steps for reaching reliable extrapolation of the pedestal performance to future machines.

The present work investigates the dependence on the dimensionless parameters ρ^*, ν^*, β of the energy confinement, of the core thermal transport, of the pedestal structure and of the pedestal stability in JET-ILW. The experimental results are qualitatively compared with the peeling-ballooning (P-B) model [Wilson PoP2002, Snyder PoP2002]. When possible, the results are compared with JET-C.

The paper is organized as follows. Section 2 describes the experimental scenario, the dataset and the main diagnostics. Section 3 describes the ρ* scaling, Section 4 the ν* scaling and Section 5 the β scaling. Conclusion are discussed in Section 6.

2. SCENARIO, DIAGNOSTICS and PARAMETERS.

2.1 SCENARIO

The scenario used for the dimensionless scans has low triangularity (δ). The low triangularity has been chosen to have a consistent comparison with the earlier dimensionless scans, where the low-δ was used. Moreover, in low β plasmas ($\beta_N \lesssim 1.8$) the JET-ILW high-δ plasmas do not show any significant difference in the confinement from the low-δ [Beurskens NF2014, de la Luna IAEA2014]. So far, a difference in the confinement between low and high δ in JET-ILW has been observed only at high β ($\beta_N \gtrsim 1.8$) in the so called "hybrid plasmas" [Challis NF2015, Maggi NF2015]. The present JET-ILW scans have been performed with the outer strike point at the divertor corner near the pump duct. This configuration allows the density control. The plasmas are heated mainly via NBI. The ICRH power is in the range 1-4MW and is used to reduce W accumulation in the core.

The present plasmas are in a Type I ELMy H-mode as suggested by the increase of the ELM frequency with the power through the separatrix. The pedestal temperature is $T_e^{ped} \geq 400eV$, while the Type III ELMs occur at $T_e^{ped} \leq 300eV$ in JET-ILW [Beurskens NF2014]. Moreover, the ELM energy losses are large compared to the Type III ELMs ($W_{ELM}/W_{ped} > 5\%$) and are consistent with Type-I energy losses [Loarte PPCF2003, Frassinetti NF2015].

2.2 MAIN DIAGNOSTICS

The High Resolution Thomson Scattering (HRTS) [Pasqualotto RSI2004] is used to measure electron temperature and density. Only the profiles in a stationary phase are considered for the analysis of the pedestal structure. The stationary phases used are longer than 0.5s and at least four energy confinement times long. The pedestal structure is determined using only the pre-ELM profiles and fitting the experimental data with a modified hyperbolic tangent function [Groebner NF2001] considering the effect of the instrument function [Frassinetti RSI2014]. The electron pressure pedestal height is determined from the temperature and density pedestal height, $p_e^{ped}=k_B \cdot T_e^{ped} \cdot n_e^{ped}$. To be consistent with the earlier experimental estimations [Leyland NF2013, Leyland NF2015] and with the definition used in the EPED model [Snyder PoP2009], the pressure width is calculated as the average between the electron temperature width and electron density width. The reflectometer data [Sirenelli RSI2010], when available, have been used to cross check the density pedestal width and position obtained with the HRTS.

The charge exchange diagnostics, when available, have been used to measure ion temperature and plasma rotation. As discussed in section 2.3, when the charge exchange was not available it is reasonable to assume $T_i=T_e$.

The effective charge Z_{eff} is a line average measurement from the visible Bremsstrahlung [Meister RSI2004]. No systematic measurement of the Z_{eff} profile is available.

The core transport has been studied using the TRANSP code [Goldston JCP1981] with the following profiles as inputs. Electron temperature and density profiles are measured with the HRTS and using $T_i=T_e$. The ion density profile is calculated to be proportional to the electron density assuming a uniform effective charge measured from the visible Bremsstrahlung [Meister RSI2004]. No systematic measurement of the Z_{eff} profile is available. The profiles of the bulk radiation are determined with a tomographic reconstruction of the bolometric measurements [Mast RSI1985].

2.3 THE DATASETS AND THE PARAMETERS FOR JET-ILW AND JET-C

The JET-ILW dimensionless scans have been performed changing the engineering parameters in order to vary one dimensionless parameter while keeping the other parameters as constant as possible. When possible, the JET-ILW data are compared with JET-C. However, only the last JET-C campaign has provided pedestal profiles with good enough quality for the study of the pedestal and of the stability. It was possible to identify a JET-C dataset for the ρ* scan, even though with some differences from the JET-ILW ρ*scan, as later described. For ν* no dimensionless scans are available from the last JET-C campaign. Therefore, for comparison with the present JET-ILW ν* scans, the low-δ/low-β ("baseline") JET-C plasmas of reference [Beurskens NF2013] are used. These JET-C shots can be considered as representative for typical low-δ/low-β plasmas obtained with the carbon wall, but only very few of them have a quality of the HRTS data good enough for the study of the pedestal structure. For the β scan, no JET-C plasmas with good pedestal data are available.

The range of variation of the main dimensionless parameters for the datasets used in this work is summarized in table 1. The dimensionless parameters are calculated using the definitions in section 1 by volume integrating dimensionless profiles. In this case, the profiles in the entire ELM cycle have been used (i.e. not the pre-ELM profiles). Note that the normalized thermal β is used ($\beta_N^{th}=\beta^{th}aB_T/I_p$). Since the scans have been performed at constant q_{95}, constant β_N^{th} implies that constant β^{th}.

In the entire dataset $T_e=T_i$ within the experimental uncertainty (<10%) both in the core and at the edge. This has been experimentally verified using the charge exchange diagnostic, when available. Moreover, the ion-electron coupling has been estimated as in reference [Beurskens NF2013] by calculating the ratio of the energy exchange time (τ_{ex}) and the energy confinement time. $\tau_{ex}/\tau_E<0.5$ for the entire datasets confirming that $T_e=T_i$. The same equilibrium has been used. $q_{95}\approx3.0$ for the entire JET-ILW dataset. JET-C has lower q_{95} for the ρ*scan ($q_{95}\approx2.6$). The effective charge is not perfectly constant with a 20-25% variation in the JET-ILW datasets and 25-30% in the JET-C ρ* scan. It was not possible to keep the Mach number perfectly constant. However, as shown in [De Vries NF2008], the dependence with M_{rot} is weak $\tau_E \propto (M_{rot})^{0.21}$. Therefore, the present variation in the Mach number should affect the energy confinement by ≈10%, much less than the experimentally observed τ_E variation. In the following analysis, the role of the Mach number is neglected for simplicity.

Specific comments for each scan will be discussed in the next sections.

parameter	ρ* scan		ν* scan	β scan	[NF2013]
	JET-ILW	JET-C	JET-ILW	JET-ILW	JET-C
<ρ*> (%)	**0.3-0.5**	**0.3-0.5**	0.40-0.45	0.40-0.45	0.40-0.47
<ν*>	0.05	0.050	**0.03-0.15**	$\begin{cases} 0.03\ (low\ \nu*\ scan) \\ 0.15\ (high\ \nu*\ scan) \end{cases}$	0.03-0.1
$<\beta_N^{th}>$	1.4-1.5	1.5-1.6	$\begin{cases} 1.8\ (scan\ 1) \\ 1.7\ (scan\ 2) \\ 1.6\ (scan\ 3) \\ 1.5\ (scan\ 4) \end{cases}$	**1.4-1.8**	1.45-1.75
$<M_{rot}>$	0.6-0.8	0.7-0.9	0.3-0.45	0.3-0.45	0.4-0.8
Z_{eff}	1.2-1.5	2.1-2.8	1.2-1.4	1.2-1.4	1.8-3.0
T_i/T_e	1.0	1.0	1.0	1.0	1.0
q_{95}	3.0	2.6	3.0	3.0	2.5-3.5

Table 1. *Summary of the dimensionless parameters used in this work. Numbers in bold highlight the range of variation for each scan. The $\rho*$, $\nu*$ β and M_{rot} parameters represents the volume average. The last column shows the parameters of the low-δ plasmas of reference [Beurskens NF2013]. The last column is not a dimensionless scan and will be used only as representative low δ JET-C plasmas for comparison with the JET-ILW $\nu*$ scan.*

3. ρ* DIMENSIONLESS SCAN.

The ρ* scan is important to determine the extrapolation of the energy confinement to ITER. While the present day machines might reach ν* and β similar to those of future experiments, comparable ρ* cannot be reached. Earlier dimensionless scalings have shown a ρ* dependence compatible with a gyro-Bohm scaling. As discussed in Section 1, there is concern that the low JET-ILW confinement so far obtained at high current might imply a weaker ρ*scaling with a metal wall.

The JET-ILW dataset used for the dimensionless ρ* scan is described in table 1. ρ* is varied from 0.3% to 0.5%. The other dimensionless parameters are constant. However, it was not possible to keep β perfectly constant and a systematic weak increase with ρ* is present. In the following figures the data with slightly higher β_N are represented with empty symbols. Due to (1) the narrow range of variation in β_N (≈10% from the ρ* columns of table 1) and (2) the weak β_N scaling at the present ν* value (see section 5), this difference does not significantly affect the result. Note that it was not possible to find a JET-C dataset perfectly consistent with the JET-ILW ρ* scan and with good pedestal data. The JET-C dataset used in this work has lower q_{95} and significantly higher Z_{eff}. So, no quantitative claims can be made on the JET-ILW / JET-C comparison in this section. Qualitative comparison are in any case useful, especially considering that no JET-C information on the role of ρ* in the pedestal stability are available.

Before discussing the global confinement, it is important to highlight that the density and temperature profiles, and hence also the dimensionless profiles, match very well.

3.1 GLOBAL CONFINEMENT AND THERMAL TRANSPORT

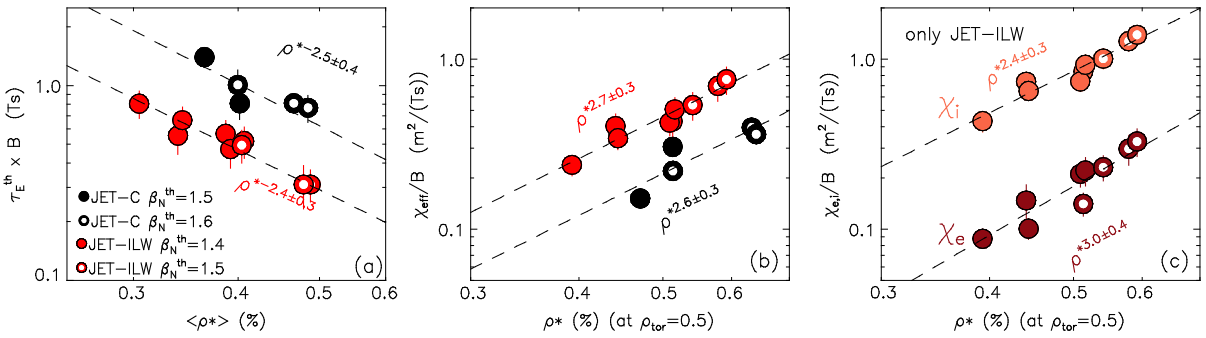

Figure 1. *(a) Normalized energy confinement versus volume averaged ρ*. (b) Normalized effective thermal diffusivity calculated at ρ_{tor}=0.5 versus local ρ* calculated at ρ_{tor}=0.5. ρ_{tor} is the square root of the normalized toroidal flux. (c) Normalized ion and electron thermal diffusivity at ρ_{tor}=0.5. The dashed lines represent the exponential fits to the experimental data.*

The dependence of the normalized energy confinement with ρ* is shown in figure 1(a). The JET-ILW normalized confinement scales as $B\tau_E \approx \rho^{*-2.4\pm0.3}$, a trend consistent, within the error bars, with the earlier JET-C estimations ($B\tau_E \approx \rho^{*-2.7}$) [Cordey NF2005]. Also the present JET-C dataset ($B\tau_E \approx \rho^{*-2.5\pm0.4}$) is in agreement with the earlier JET-C estimation.

The thermal diffusivity has been calculated using interpretative TRANSP simulations, with the experimental inputs described in section 2.2. More details can be found in reference [Kim NF2015]. Due to the uncertainty in the experimental temperature profiles it is difficult to obtain an accurate estimation of the equipartion term and hence of the ion and electron thermal diffusivities separately. Therefore, the effective thermal diffusivity χ_{eff} is used, where χ_{eff} is defined as:

$$\chi_{eff} = \frac{q_e + q_i}{n_e \nabla T_e + n_i \nabla T_i} \tag{7}$$

with q_e and q_i the electron an ion heat fluxes respectively. The trend of the normalized χ_{eff} with ρ* is shown in figure 1(b). A strong reduction of the thermal diffusivity with decreasing ρ* is observed. The exponents are 2.7±0.3 for JET-ILW and 2.6±0.3 for JET-C, consistent with earlier results and with a core transport consistent with a gyro-Bohm scaling. Even if less reliable due to the uncertainty in calculating separately the ion and electron heat fluxes, the trend with ρ* of χ_e and χ_i for the JET-ILW dataset are shown in figure 1(c). The exponents are ≈2.4±0.3 for χ_i and ≈3.0±0.4 for χ_e, suggesting a gyro-Bohm transport for the electrons.

This difference in the thermal transport scaling between ions and electron is consistent with the DIII-D results in L-mode [Petty PRL1995].

In conclusion, despite the fact that JET-ILW has not reached yet H_{98}=1 at high current, the metal wall does not seem to have modified the scaling with ρ* in low δ baseline plasmas. Obviously, in the ρ* scan it is essential to keep ν* and β constant to achieve this conclusion. H_{98}=1 has not been reached yet in high I_p JET-ILW plasmas not because of a different ρ* scaling, but because of the lower β and higher ν* obtained in comparison to JET-C.

3.2 PEDESTAL STRUCTURE AND STABILITY

The pedestal structure is studied in terms of pedestal width and normalized pressure gradient. The pressure pedestal width versus ρ* is shown in figure 2(a). Within the error bars, no clear trend with ρ* is observed both in JET-C and in JET-ILW. This is in agreement with the high triangularity plasmas obtained in JET-C and in DIII-D and described in references [Beurskens PPCF2009, Beurskens PoP 2011].

No information on the dependence on ρ* of the experimental normalized pressure gradient are available in literature. This dependence is important for two reasons. First of all, the trend of the normalized pressure gradient with ρ*, combined with the information on the pedestal width, can provide information for an extrapolations of the pedestal height to ITER. Second, the experimental normalized pressure gradient can be compared with the results of the P-B stability in order to verify if the present theorical model can reliably predict the pedestal behaviour with ρ*. The normalized pressure gradient α is defined as [Miller PoP1998]:

$$\alpha = -\frac{2\partial_\psi V}{(2\pi)^2}\left(\frac{V}{2\pi^2 R}\right)^{1/2}\mu_0 p' \qquad (8)$$

with V the plasma volume, R the major radius and p' the pressure derivative in the poloidal flux ψ. From a practical point of view, α is proportional to the pressure gradient divided by I_p^2. The experimental normalized pressure gradient, α_{exp}, has been calculated using the fits to the experimental profiles. The dependence of α_{exp} with ρ* is shown in figure 2(b). Both for JET-C and JET-ILW, no dependence of α_{exp} is observed within the scatter of data. The importance of this result will be discussed at the end of the section.

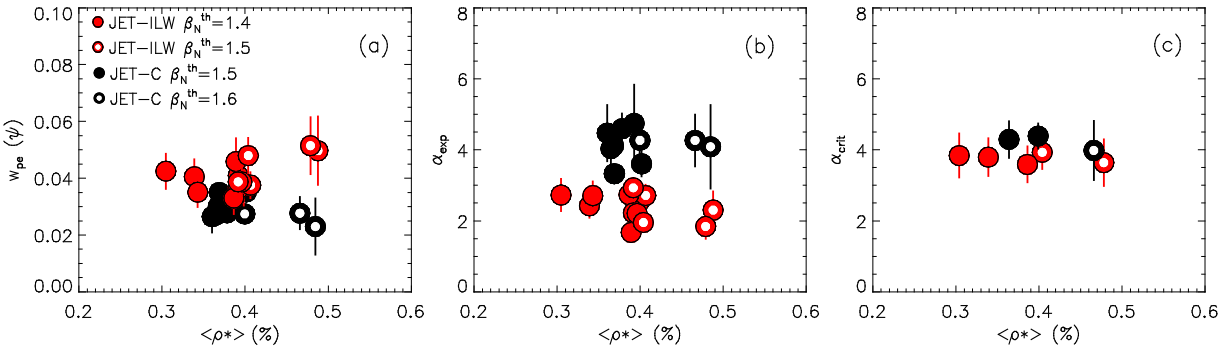

Figure 2. *(a) Pedestal pressure width (in normalized poloidal flux unit) (b) Experimental normalized pressure gradient versus ρ*. (c) theoretical α_{crit} (calculated from the intersection of the P-B stability boundary with the self-consistent path in the j-α space) versus ρ*.*

The comparison of the experimental results with the theory is done using the peeling-ballooning (P-B) model [Wilson PoP2002, Snyder PoP2002]. The pedestal stability of the experimental plasmas has been studied using ELITE to obtain the *j*-α stability diagram, where *j* is the current density and α the normalized pedestal pressure gradient. The equilibrium is calculated using the HELENA code [Huysmans CP1991]. The fits to the experimental T_e and n_e profiles selected in the pre-ELM phase are used. The JET-ILW results show that in this datset the operational points are far from the P-B stability boundary. This behaviour is relatively common in JET-ILW and it has been systematically observed in high-gas/low-β plasmas [Beurskens NF2014, Maggi NF2015, Leyland NF2015, Nunes EPS2016]. The discrepancy has not been yet understood and it is currently under investigation. Despite this problem, it is still useful to investigate the results of the P-B model in order to have a qualitatively comparison with experimental results.

The stability boundaries are not drastically modified by ρ*. To quantify this claim, the critical normalized pressure gradient (α_{crit}) has been calculated. α_{crit} represents the normalized pedestal pressure expected by the P-B model and it is determined by the intersection of the self-consistent path of the operational point in the *j*-α space with the stability boundary. The self-consistent path is determined as described in [Saarelma PoP2015] by increasing height of the pedestal temperature and then self-consistently calculating the current profile in order to find the marginally stable pedestal temperature height. α_{crit} has been calculated foe a subset of the data shown in figures 2(a) and 2(b). The result show no trend of α_{crit} versus ρ* and hence no dependence of the pedestal stability with ρ*. Note that, for the JET-C dataset, α_{exp} and α_{crit} are comparable. This is is consistent with earlier JET-C analysis that shows the operational point close to the P-B boundary [Beurskens NF2013].

In conclusion, the pedestal stability does not show any significant dependence with ρ*. This has two implications. First of all, it implies that the ITER pedestal stability will not be negatively affected by the low ρ* operation. Second, since $\rho^* \sim T_i^{0.5}/I_p$ (at contant q_{95}) and since $\alpha_{exp} \sim \nabla p_e / I_p^2$, it confirms that the high current operation can be very effective in achieving a high pressure gradient and hence a high pedestal pressure.

4. ν* DIMENSIONLESS SCAN.

The results of the first JET-ILW campaign [Beurskens NF2014] have shown that the JET-ILW low δ baseline plasmas tend to reach confinement close to the corresponding JET-C plasmas at low collisionality. The origin of the improvement was only partially understood. In references [de la Luna IAEA2014, Maggi NF2015] it is discussed that the reduced ν* leads to an improvement of the core stored energy via the T_e profile stiffness and via the increase in density peaking [Weisen PPCF2006]. These plasmas were characterized by different β and ρ*, so strong conclusions on the role of ν* were not possible.

This section discusses the role of ν* on the confinement and on the pedestal stability in JET-ILW. Four ν* scans have been analysed, each one with a different β_N. ρ* is constant in the entire dataset. No recent dimensionless ν* scan is available for JET-C. So, the JET-C low-δ / low-β plasmas described in reference [Beurskens NF2013] will be used. These shots were considered as representative good performance JET-C plasmas. Unfortunately, very few of them have good pedestal data.

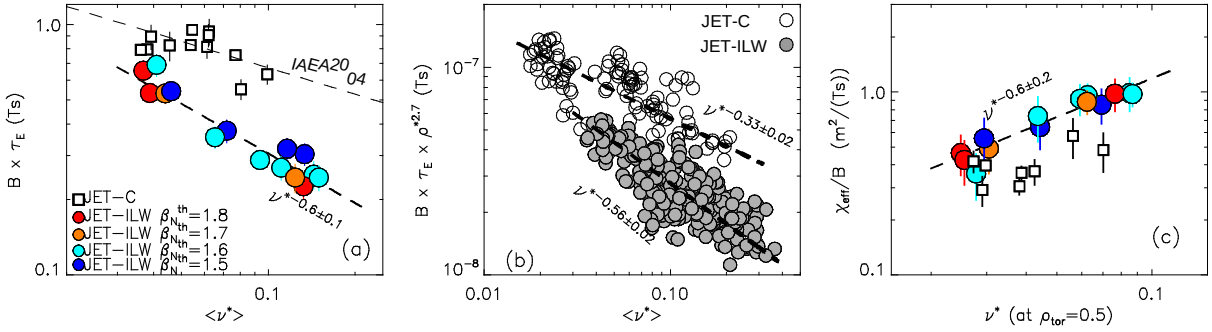

Figure 3. *(a) normalized energy confinement versus volume averaged ν*. The thick dashed line is a fit to the JET-ILW data. The thin dashed line shows the trend $B\tau_E \propto \nu^{*-0.35}$ determined in [McDonald IAEA2004]. (b) normalized energy confinement with the ρ* dependence removed for the entire dataset used in reference [Beurskens NF2014] (c) normalized effective thermal diffusivity calculated at ρ_{tor}=0.5 versus local ν* calculated at ρ_{tor}=0.5. The thick dashed lines represents the exponential fits to the JET-ILW experimental data.*

4.1 GLOBAL CONFINEMENT AND THERMAL TRANSPORT

The trend of the normalized energy confinement versus ν^* is shown in figure 3(a). A strong improvement of the confinement is observed with decreasing ν^* for the JET-ILW dataset. The scaling exponent is $\alpha_\nu \approx 0.6$. For comparison, the earlier JET-C trend with $\alpha_\nu \approx 0.35$) is shoiwn as well [Mc Donald IAEA2004]. A dependence with ν^* stronger in JET-ILW than in JET-C is observed. This leads to reduction in the difference between JET-C and JET-ILW confinement from ≈40% at high ν^* to ≈10% at low ν^*. To strengthen the result, figure 3(b) shows the correlation between the normalized energy confinement and ν^* for the entire JET-C and JET-ILW datasets used in [Beurskens NF2014]. These discharges were not a dimensionless scan, so the ρ^* dependence has been removed. For simplicity, the β dependence has not been considered (the normalized confinement in JET-C has no β dependence [Mc Donald PPCF2004] and in JET-ILW the dependence is present only at very high $\nu*$, as discussed in Section 5) . The result shows that $\alpha_\nu \approx 0.33$ in JET-C, consistent with the results described in [MdDonald IAEA2004], while $\alpha_\nu \approx 0.56$ in JET-ILW, consistent with the estimation of figure 3(a). Note that the JET-ILW data of the dimensionless scan shown in figure 3(a) are not included in the dataset of figure 3(b).

In the core, a strong reduction of the core thermal transport is observed with decreasing ν^*, figure 3(c). This positive dependence implies that the core transport is between a transport driven by collisionless ITG and trapped electron modes (which expects $\alpha_\nu=0$) [Waltz PoP1997] and to a transport driven by resistive ballooning modes (which expects $\alpha_\nu=1$) [Hassam PF1992]. However, resistive ballooning modes are localized near the plasma edge. This might suggest a possible correlation of the core temperature with the edge temperature. Indeed, the temperature profile is relatively stiff and no strong trend of the temperature peaking with ν^* is observed, as already noted in [Frassinetti NF2016]. On the other hand, part of the increase in the core stored energy is due to the increase in the density peaking, as typically observed in most of the tokamaks [Angioni PoP2002, Maslov NF2009, Valovic PPCF2005, Weisen PPCF2006].

4.2 PEDESTAL STRUCTURE AND STABILITY

The strong increase of the normalized global confinement with decreasing ν^* and the correlation between core and pedestal stored energy shown in figure 3 motivate the study of the pedestal structure dependence with ν^*. Note that since the density peaking changes with ν^*, the dataset of figure 3 does not have perfectly constant pedestal ρ^* and pedestal β. Therefore, a slightly different dataset, with constant ρ^{*ped} and β^{ped}, is considered in this

section. Initially, we will focus only on the JET-ILW datasets. The JET-C results are discussed at the end of this section.

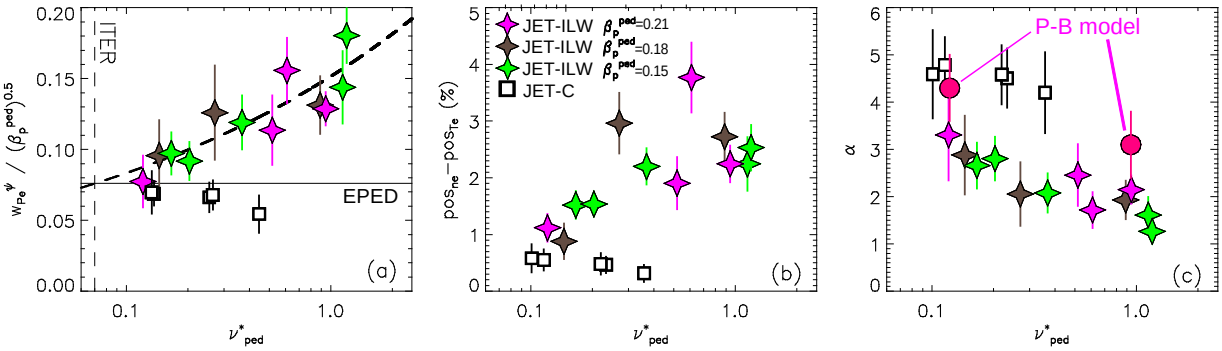

Figure 4. *(a) pedestal width normalized to the square root of the β_p^{ped} versus ν^*_{ped}. The horizontal line shows the value used in EPED. The thick dashed line shows a power law fit to the experimental data. (b) Relative shift between the density and temperature pedestal position versus ν^{*ped}. (c) Normalized pressure gradient versus ν^*_{ped}. The circles represent the α_{crit}.*

The dependence of the pedestal width with the pedestal ν* is shown in figure 4(a). The width has been normalized to remove the beta dependence. The empirical beta dependence $w_{\mathrm{pe}} = 0.076\sqrt{\beta_p^{ped}}$ determined in [Snyder PoP2009] and implemented in the EPED model is used. β_p^{ped} is the poloidal beta at the pedestal. As discussed in reference [Frassinetti NF2016], an increase of the pedestal width with increasing ν* is observed in JET-ILW. The reason is still under investigation, but the result is consistent with what observed recently in JT-60U [Urano NF2016]. Note that, at low ν*, no significant deviation from the empirical scaling described in [Snyder PoP2009] is observed. Moreover, an extrapolation of the experimental fit to low ν* values suggests that the trend has no major influence for the ITER pedestal width.

A second significant difference in the pedestal structure is the position of the pedestal density relative to the position of the pedestal temperature. Hereafter, the difference between the n_e pedestal position and the T_e pedestal position is called simply "relative shift". The relative shift versus ν* is shown in figure 4(b). A decrase of the relative shift with decreasing ν* is observed in the JET-ILW dataset.

The experimental normalized pressure gradient α_{exp} is shown in figure 4(c). An increase of α_{exp} with decreasing ν* is observed in the JET-ILW scans, suggesting an improvement of the pedestal stability at low ν*. This is confirmed with the P-B model by calculating α_{crit} for a low and a high ν* plasma. The trend of α_{crit} with ν* is qualitative similar to the experimental trend. The improvement of the stability is due to three factors. (1) the reduction of ν* leads to the increase of the bootstrap current which in turn moves the intersection of the self-consistent

path with the stability boundary to higher α. (2) the decrease of the pedestal width with decreasing ν^* has a stabilizing effect [Snyder NF2011] hence slightly moving the stability boundary to higher α. (3) A further reason, described in detail in reference [Stefanikova EPS2016], is related to the reduction of the relative shift. This has three effects: first of all, it reduces the collisionality in the pedestal region hence increasing the bootstrap current. Second, it affects the shape of the pressure profile increasing the gradient and leading to a further increase in the bootstrap current. Third, it slightly moves the pedestal pressure inwards producing a further stabilizing effect [Saarelma PoP2015]. A change in the relative shift was already observed in DIII-D [Beurskens PoP2011], but it was related to ρ^* (note that, so far, no clear trend of the shift with ρ^* has been observed in JET-ILW). Recently, the increase in the confinement due to lithium seeding in DIII-D has been correlated to the reduction of the relative shift (more precisely to an inward shift of the density) [Osborne NF2015].

The behavior of the pedestal stability with collisionality might suggest an explanation for the difference in the scaling of the normalized confinement versus ν^* observed in JET-C and JET-ILW [figure 3(a) and 3(b)]. However, we must highlight that conclusive claims on the origin of the difference are still not possible because the JET-C dataset is not a dimensionless ν^* scan and because it has only five shots with good pedestal profiles. In any case, we can observe a clear difference. First of all, the pedestal width and relative shift of the JET-C dataset are not affected by collisionality, figure 4. Therefore, a weaker improvement of the pedestal with decreasing ν^* is expected in the JET-C dataset. Indeed, the trend of α_{exp} with ν^* is much weaker in the JET-C dataset than in the JET-ILW dataset, figure 4(c). So, we might speculate that the stronger trend of the normalized confinement with ν^* in JET-ILW is related to the stronger improvement in the pedestal stability with decrasing ν^*.

The correlation between the relative shift and the collisionality might suggest a role of the atomic physics in the pedestal stability. The dimensionless collisionality scan is in fact achieved by varying the power, the current and the gas rate. It is possible that the increased gas level influences the density pedestal position. However, conclusive claims on what drives the change in the relative shift shown in figure 4(b) are not possible at the moment. Initial experimental results show that the relative shift is in fact influenced by both the gas and the power [Stefanikova EPS2016]. This topic is now under intensive investigation and will be the subject of future works. A further discussion is presented in Section 6.

5. β DIMENSIONLESS SCAN.

The earlier β dimensionless scans have produced contradicting results. In JET-C and DIII-D it is shown a negligible dependence of the normalized energy confinement with β [McDonald PPCF2004, Petty PoP2004], while in JT-60U and ASDEX Upgrade a reduction with increasing β was observed [Urano NF2006, Vermare NF2007]. The β dimensionless scans presented in this section show that in JET-ILW both behaviours can be observed. The dataset used is a subset of the ν* dataset obtained by selecting the shots with lowest ν* (labelled "low ν* scan" in table 1) and with highest ν* (labelled "high ν* scan" in table 1). In both cases, the β range is not large, from $\beta_N^{th}\approx1.4$ to $\beta_N^{th}\approx1.8$, but it is sufficient to extract useful information. No JET-C plasmas useful for a comparison are available.

5.1 GLOBAL CONFINEMENT AND THERMAL TRANSPORT

The normalized energy confinement versus β is shown in figure 5(a). At low ν*, the normalized energy confinement seems not dependent on β_N^{th}. However, due to the limited range in β the uncertainty on the scaling exponent is large, α_β=-0.1±0.4. On the other hand, at high ν* a clear reduction of the normalized confinement with increasing β_N^{th} is observed. The corresponding scaling exponent is α_β=1.2±0.6.

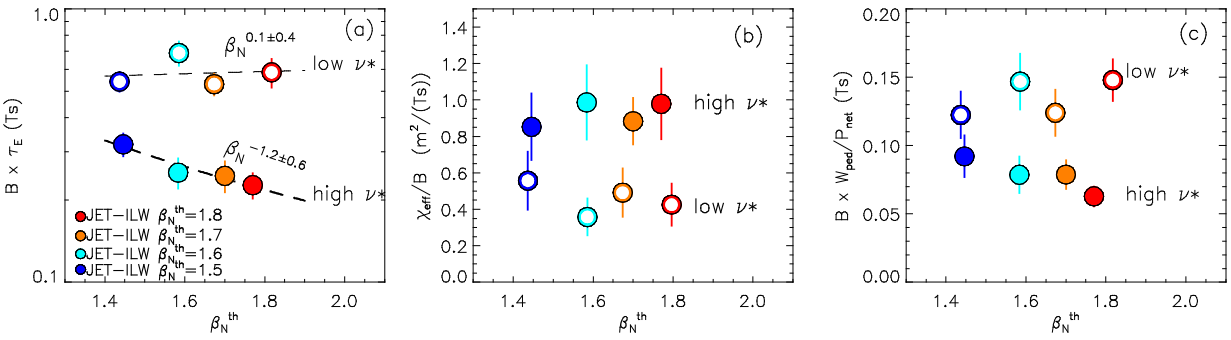

Figure 5. *(a) normalized energy confinement versus β_N^{th}. (b) effective thermal diffusivity versus β_N^{th}. (c) estimation of the normalized pedestal energy confinement. versus β_N^{th}. The empty symbols correspond to the low ν* scan (ν*≈0.03) and the full symbols to the high ν* scan (ν*≈0.15).*

The analysis of the core thermal diffusivity shows that this different behaviour at high and low ν* is not related to a difference in the core heat transport. The effective thermal diffusivity is shown in figure 5(b). Within the error bars, no trends with β_N^{th} are observed. The lack of strong dependence of the thermal diffusivity with β_N^{th} suggests that, in these β_N ranges, the core turbulent transport is dominated by electrostatic effects (see section 1).

The degradation of the normalized confinement with β_N^{th} at high ν* is driven by the pedestal. In figure 5(c), a proxy for the normalized pedestal energy confinement is shown.

The proxy for the pedestal energy confinement is estimated as the pedestal stored energy divided by the total heating power. The results shows a clear reduction of normalized pedestal energy confinement with increasing β_N^{th} at high ν*.

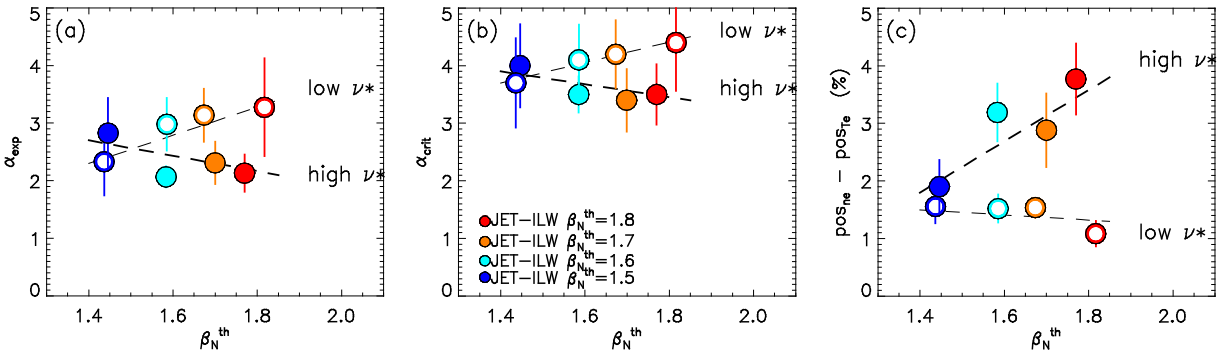

Figure 6. *(a) experimental normalized pressure gradient versus β_N^{th}. (b) critical normalized pressure gradient determined from the P-B stability versus β_N^{th}. (c) relative shift between pedestal position of electron density and electron temperature versus β_N^{th}. The empty symbols correspond to the low ν* scan (ν*≈0.03) and the full symbols to the high ν* scan (ν*≈0.15).*

5.2 PEDESTAL STABILITY

To understand the different trends with β_N^{th} at low and high ν*, the results of the stability analysis have been compared to the experimental normalized pedestal gradient. The experimental normalized pressure gradient is shown in figure 6(a). At low ν*, an increase of α_{exp} with increasing β_N^{th} is observed, while at high ν* a reduction of α_{exp} with β_N^{th} is present. The results of the stability analysis are summarized in figure 6(b), where the critical α versus β_N^{th} is shown. The α_{crit} trends determined with the P-B stability analysis are qualitatively consistent with the experimental trends. At low ν* the increase of α_{crit} with increasing β_N^{th} is observed. This result is expected, since it is well know that the increase of β improves the pedestal stability via the increase of the Shafranov shift. On the contrary, the opposite trend is present at high ν* , where a reduction of α_{crit} with increasing β_N^{th} is observed. This result is not expected and shows that, in the high ν* scan, the stability is affected not only by β but also by another mechanism. This is discussed in figure 6(c), where the relative shift between the position of the pedestal density and the temperature is shown. A clear difference between the low ν* scan and the high ν* scan is observed. While at low ν*, the relative shift does not change significantly with β_N^{th}, at high ν*, the relative shift tends to increase with increasing β_N^{th}. As discussed in section 4, the increase of the relative has a strong destabilizing effect that leads to the reduction of α_{crit}.

Note that the experimental α is lower than α_{crit}. So, like for the ρ^* and the ν^* scan, the operational point is far from the stability boundary. Nonetheless, it is remarkable that the qualitative trends of α_{exp} and α_{crit} are similar.

As a final comment, probably due to the small range in β, no significant trends of the pedestal width are observed with β_N^{th}.

6. DISCUSSION AND CONCLUSIONS.

The work has investigated the dependence of normalized confinement, core thermal heat diffusivity and pedestal stability with the dimensionless parameters ρ^*, ν^* and β.

The analysis of the dimensionless ρ^* scan shows that the change from the carbon wall to the metal wall in JET has not modified the ρ^* scaling. The JET-ILW scaling exponent is, within the error bars, consistent with the earlier JET-C estimations and with a gyro-Bohm scaling. This shows that the extrapolations of the energy confinement to low ρ^* for ITER-relevant predictions remain unchanged. Moreover, it is observed that ρ^* does not affect the pedestal stability. This implies that the ITER pedestal stability will not be negatively affected by the low ρ^*.

The analysis of the dimensionless ν^* scan in JET-ILW shows an increase of the normalized energy confinement with decreasing ν^*. The earlier JET-C results have a weaker dependence. The strong dependence with ν^* in JET-ILW is related to an improvement in the pedestal stability. The P-B stability analysis shows that the improvement is due to three factors: (i) the increase of the bootstrap current, (ii) the reduction of the pedestal width and (iii) the reduction of the relative shift. The origin of the shift is still unclear and is currently under investigation. At the moment it is not possible to predict the behaviour of the relative shift. It is possible that the decrease of the relative shift with decreasing ν^* saturates at very low ν^*. This consideration suggests that it is not obvious how to extrapolate the collisionality scaling to low ITER-relevant ν^*.

The analysis of the dimensionless β scan in JET-ILW shows two different behaviours depending on the collisionality. At low ν^*, the normalized energy confinement has no clear dependence with β. The result is in agreement with earlier JET-C and DIII-D scalings. A degradation with increasing β is observed at high ν^*, in agreement with JT-60U and ASDEX-Upgrade. Note that both the JT60-U and ASDEX-Upgrade results were perfomed with relatively high ν^*. In [Vermare NF2007] it was suggested that the negative β dependence might have been related to the edge plasma. The present JET-ILW results tend to corroborate

this ASDEX-Upgrade observation. In fact, the degradation of the JET-ILW normalized confinement with increasing β at high ν* is due to the reduction of the pedestal confinement, not to an increase in the core transport (figure 5). This result stresses the importance of studying both the core and the pedestal confinement when investigating dimensionless scaling and not simply the global energy confinement.

The physics of the present two β scans might be correlated to the physics of the power scans obtained with three different gas levels discussed in references [Challis NF2015, Maggi NF2015]. In [Challis NF2015, Maggi NF2015] it was observed that the rate of increase of β_N with power was lower at high D_2 gas rate than at low D_2 gas rate. Basically, at constant power, the increase of the gas rate led to a reduction of the pedestal temperature, to a reduction of the confinement and to an increase of collisionality. The role of neutral was discussed as a possible reason for this effect. We can speculate a correlation with the results described in the present β scans. The increase of the gas rate in [Maggi NF2015] might have led to an increase of the relative shift and hence to the reduction of the pedestal stability.

We have to highlight that the origin of the increase of the pedestal relative shift is not clear yet. The result of figure 4(b) suggests a correlation with the collisionality while the result at high ν* of figure 6(c) suggests a correlation with β_N. This is roughly consistent with the results in reference [Stefanikova EPS2016], where a correlation of the relative shift with both the gas and the power is observed.

Assuming that the relative shift is driven by the increased gas, this work shows that the neutrals might play an important role in the pedestal stability and that they might affect the dimensionless scaling exponents. To bypass the problem, this work has determined the scaling exponents looking also at the thermal diffusivity in the core (where the neutrals should not play any major role). The exponents determined using the thermal diffusivity are actually in agreement with those determined with the global energy confinement, showing that the exponents determined in this work are likely not largely affected by the neutrals. The only clear exception is in the β scan at high ν*, where the exponent determined from the global confinement is largely influenced by the pedestal confinement which, in turn, is strongly affected by the change in the pedestal relative shift and, possibly, by atomic physics.

As a final comment, it is remarkable that the P-B stability analysis shows qualitative trends consistent with the experimental results in all the dimensionless scalings. This shows that the P-B model is able to correctly reproduce at least a part of the physics that determines the pedestal stability. The quantitative disagreement is still under investigation. A possibility is that the present model does not consider kinetic effects such as those related to the ion

diamagnetic drift. The kinetic effects might affect the stability of an ideal ballooning mode [Hastie PoP2003] and move the stability boundary closer to the operational point [Aiba NF2012].

ACKNOWLEDGEMENT

This work has been carried out within the framework of the EUROfusion Consortium and has received funding from the Euratom research and training programme 2014-2018 under grant agreement No 633053. The views and opinions expressed herein do not necessarily reflect those of the European Commission

REFERENCES

[Aiba NF2012] Aiba N and Oyama N, Nucl. Fusion 52 114002 (2012)
[Angioni PoP2002] Angioni C et al., Phys Plasmas **12** 112310 (2005)
[Beurskens PPCF2009] M.N.A. Beursknes et al., Plasma Phys. Control. Fusion **51** 124051 (2009)
[Beurskens PoP2011] M.N.A. Beursknes et al., Phys. Plasmas **18** 056120 (2011)
[Beurskens NF2013] M. Beurskens et al., *Nucl. Fusion* **53** 013001 (2013)
[Beurskens NF2014] Beurskens M et al., *Nucl. Fusion* **54** 043001 (2014)
[Challis NF2015] Challis C et al., *Nucl. Fusion* **55** 053031 (2015)
[Connor NF1977] Connor JW and Taylor JB, *Nucl. Fusion* **17** 1047 (1977)
[Cordey NF2005] Cordey JG et al., *Nucl. Fusion* **45** 1078 (2005)
[de la Luna IAEA2014] E. de la Luna et al. *Proc. 25th Int. Conf. on Fusion Energy (Saint Petersburg, 2014)* EX/P5-195
[de Vries PPCF2006] de Vries P.C. et al Plasma Phy. Controll. Fusion 48 1693 (2006)
[de Vries NF2008] de Vries P.C. et al Nucl. Fusion 48 065006 (2008)
[Falchetto PRL2004] Falchetto G et al., Phys. Rev. Lett. **92** 025002 (2004)
[Frassinetti NF2015] L. Frassinetti et al., Nucl. Fusion 55 023007 (2015)
[Frassinetti RSI2012] L. Frassinetti, et al., Rev. Sci. Instrum. **83**, 013506 (2012)
[Giroud NF2015] Giroud C., Plasma Physics and Control. Fusion **57** 035004 (2015)
[Goldston JCP1981] Goldston R et al., J. Comput. Phys. **43**, 61 (1981)
[Greenwald PPCF1998] Greenwald M et al., Plasma Physics and Control. Fusion **40** 789 (1998)
[Groebner NF2001] R.J. Groebner et al., Nucl. Fusion 41 1789 (2001)
[Hassam PF1992] Hassam AB et al., Phys. Fluids B **4** 1846 (1992)
[Hastie PoP2003] Hastie R.J., Ramos J.J. and Porcelli F. Phys. Plasmas **10** 4405 (2003)
[Huysmans CP1991] Huysmans G.T.A. et al, Computational Physics: Proc.Int. Conf. (Amsterdam, The Netherlands, 1991) (Singapore: World Scientific)
[ITER NF1999a] ITER Physics Basis 1999 *Nucl. Fusion* **39** 2137 (1999)
[ITER NF1999b] ITER Physics Basis 1999 *Nucl. Fusion* **39** 2175 (1999)
[Kadomstev SJPP1975] Kadomstev BB, Sov. J. Plasmas Phys. **1** 295 (1975)
[Kaye PPCF2006] Kaye SM et al., Plasma Phys. Control. Fusion **48** A429 (2006)
[Kim NF2015] Kim Y-T et al., Nucl. Fusion **57** 065002 (2015)
[Leyland NF2013] M. Leyland et al., Nucl. Fusion **53** 083028 (2013)
[Leyland NF2015] M. Leyland et al., Nucl. Fusion **55** 013019 (2015)
[Loarte, PPCF2003] Loarte et al., Plasma Phys. Control. Fusion 45 1549 (2003)
[Luce PPCF2008] Luce TC et al., Plasma Physics and Control. Fusion **50** 043001 (2008)
[Maggi NF2015] Maggi C et al., Nucl. Fusion **55** 113031 (2015)
[Maslov NF2009] M. Maslov et al., Nucl. Fusion **49** 075037 (2009)
[Mast RSI1985] Mast K., et al., Rev. Sci. Instrum. **56**, 969 (1985)
[McDonald PPCF2004] McDonald D et al., Plasma Physics and Control. Fusion **46** A215 (2004)
[McDonald IAEA2004]. McDonald et al., 20th IAEA Fusion Energy Conference (Vilamoura, Portugal) EX6-6.
[Meister RSI2004] Meister H et al., Rev. Sci. Instrum. **75**, 4097 (2004)
[Nunes NF2013] Nunes I et al., *Nucl. Fusion* **53** 073020 (2013)
[Nunes PPCF2016] Nunes I, Plasma Physics and Control. Fusion **58** 014034 (2016)
[Osborne NF2015] Osborne T. et al., Nucl. Fusion **55** 063018 (2015)
[Pasqualotto RSI 2004] R. Pasqualotto, et al., Rev. Sci. Instrum. 75, 3891 (2004). [Petty PoP1995]
[Petty PRL1995] Petty CC et al., Phys. Rev. Lett. **74** 1763 (1995)

[Petty PoP1995] Petty CC et al., Phys. Plasmas **2** 2342 (1995)
[Petty NF1997] Petty CC et al., Phys. Plasmas **37** 1 (1997)
[Petty PoP1999] Petty CC et al., Phys. Plasmas **6** 909 (1999)
[Petty PoP2004] Petty CC et al., Phys. Plasmas **11** 2514 (2004)
[Ryter IAEA1996] Ryter F et al., Fusion energy conference 1996 (Montreal), vol. 1, 625 (1997)
[Ryter IAEA1998] Ryter F et al., Fusion energy conference 1996 (Montreal), vol. 1, 625 (1997)
[Saarelma PoP 2015] Saarelma S. et al., Phys. Plasmas **22** 056115 (2015)
[Sauter PoP2002] Sauter O et al., Phys Plasmas **9** 5140 (2002)
[Shirai PPCF2000] Shirai H et al., Plasma Physics and Control. Fusion **42** 1193 (2000)
[Sirinelli RSI 2010] A. Sirinelli, B. Alper, C. Bottereau, et al., Rev. Sci. Instrum. 81, 10D939 (2010)
[Snyder PoP2002] Snyder PB et al., Phys. Plasmas **9** 2037 (2002)
[Snyder PoP2009] P.B. Snyder et al., Phys. Plasmas **16** 056118 (2009)
[Snyder NF2011] P.B. Snyder et al., Nucl. Fusion **51** 103016 (2011)
[Stefanikova EPS2016] E. Stefanikova, 43rd EPS Conf. On Plasma Physics (Leuven, Belgium) O4.117
[Urano NF2006] Urano H et al., *Nucl. Fusion* **46** 781 (2006)
[Urano NF2016] Urano H et al., *Nucl. Fusion* **56** 016005 (2016)
[Valovic PPCF2004] Valovic M. et al., Plasma Phys. Control. Fusion 46 (2004)
[Valovic NF2011]] Valovic Nucl. Fusion **51** 073045 (2011).
[Vermare NF2007] Vermare Nucl. Fusion **47** 490 (2007).
[Weisen PPCF2006] Weisen H. et al., Plasma Phys. Control. Fusion 48 A457 (2006)
[Waltz PoP1997] Waltz RE et al., Phys. Plasmas **4** 2482 (1997)
[Wilson PoP2002] Wilson P et al., Phys. Plasmas **9** 1277 (2002)